# 8 Superconductivity and Magnetism

D.G. Eshchenko, P.S. Häfliger (April 2006 to March 2007), H. Keller, R. Khasanov, I. Landau (November till December 2006), F. La Mattina, A. Maisuradze, J. Roos, S. Strässle, St. Weyeneth, B.M. Wojek (since December 2006), R. Kuhn (Master student), C. Duttwyler (Master student)

Visiting scientists:
M.V. Eremin, B. Graneli, A. Ivanshin, B. Kochelaev, R. Pusniak, A. Shengelaya

Emeritus members:
Prof. K.A. Müller (Honorarprofessor), Prof. T. Schneider (Titularprofessor), Dr. M. Mali

*in collaboration with:* ETHZ (K. Conder, J. Karpinski), PSI (K. Conder, E. Morenzoni), Max-Planck-Institute for Solid State Research Stuttgart (A. Bussmann-Holder), IBM Rüschlikon Research Laboratory (J.G. Bednorz), University of Geneva (Ø. Fischer, J.M. Triscone), University of Birmingham (E.M. Forgan), University of Rome (D. Di Castro), Kazan State University (A. Dooglav, M.V. Eremin, V. Ivanshin, B.I. Kochelaev), Polish Academy of Sciences (R. Puzniak), University of Belgrade (I.M. Savić), Tbilisi University (A. Shengelaya), Kurchatov Institute (V.G. Storchak), University of Tokyo (T. Sasagawa, H. Takagi), UBC (J.H. Brewer), Iowa State University (A. Kaminski).

In 2006 we continued our research on magnetic and electronic properties of novel materials which we investigated by means of a combination of different complementary experimental techniques, including muon spin rotation ($\mu$SR), electron paramagnetic resonance (EPR), nuclear magnetic resonance (NMR), nuclear quadrupole resonance (NQR), as well as SQUID and torque magnetometry.

The main research topics were:

- Study of magnetic and electronic properties of novel superconductors: magnetic penetration depth in cuprate high-temperature superconductors and its signature of a two-gap behavior, local magnetic fields in cuprate multilayers studied by $\mu$SR, rare-earth ion relaxation in YBCO compounds by EPR, charge fluctuation effects in YBCO compounds by NMR/NQR, magnetic penetration depth studies in non-centrosymmetric superconductors $Li_2(Pd/Pt)_3B$ by $\mu$SR, magnetization studies of Al doped $MgB_2$.
- Investigation of the oxygen isotope effect and its field dependence in cuprate high-temperature superconductors.
- Pressure effect on the Ginzburg-Landau parameter in $YB_6$.
- Investigations of electric-field effects on the electronic structure of Cr-doped strontium titanate.
- Exploration of the microscopic magnetic properties of dilute magnetic semiconductor films by low-energy $\mu$SR.

## 8.1 Studies of oxygen isotope effects in novel superconductors

### 8.1.1 Oxygen isotope effect in optimally doped high-temperature superconductors

The observation of unusual isotope effects in cuprate high-temperature superconduc-

tors (HTS) on the transition temperature $T_c$ (see e.g. (1; 2)) and on the zero temperature in-plane magnetic penetration depth $\lambda_{ab}(0)$ (see e.g. (3; 4; 5; 6; 7)) poses a challenge to the understanding of high temperature superconductivity. It was found that the oxygen isotope ($^{16}O/^{18}O$) effect (OIE) on both $T_c$ and $\lambda_{ab}(0)$ have a tendency to increase with decreasing doping (3; 4; 5; 6; 7). In particular, for different families of cuprate HTS there is a *universal* correlation between the isotope shifts of these two quantities (5; 6; 7). Namely, in the under-doped region $\Delta T_c/T_c$ and $\Delta\lambda_{ab}(0)/\lambda_{ab}(0)$ scale linearly with respect to each other with $|\Delta T_c/T_c| \simeq |\Delta\lambda_{ab}(0)/\lambda_{ab}(0)|$. However, close to optimal doping the situation is not so clear. The Zürich group (5; 6) observed that in optimally doped $YBa_2Cu_3O_{7-\delta}$ the small OIE on $T_c$ is associated with a rather large isotope shift of $\lambda_{ab}$, even comparable with that found in under-doped cuprates. In contrast, Tallon *et al.* (7) showed that in slightly over-doped $La_{2-x}Sr_xCu_{1-y}Zn_yO_4$ the OIE on $\lambda_{ab}(0)$ is zero while the OIE on $T_c$ remains still substantial.

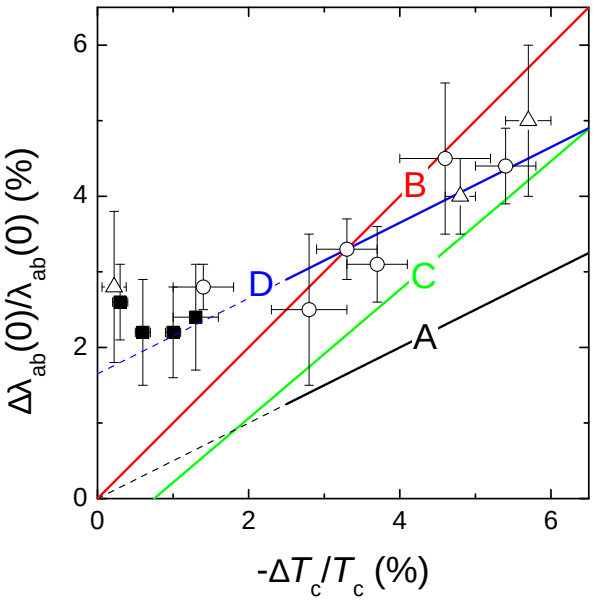


**Figure 8.1: Plot of the isotope shift $\Delta\lambda_{ab}(0)/\lambda_{ab}(0)$ versus the isotope shift $-\Delta T_c/T_c$. Full squares are the $\mu$SR data obtained for $YBa_2CuO_{7-\delta}$, $Y_{0.8}Pr_{0.2}Ba_2Cu_3O_{7-\delta}$, $YBa_2Cu_4O_8$ and $La_{1.85}Sr_{0.15}CuO_4$. Circles are bulk $\mu$SR data for $Y_{1-x}Pr_xBa_2Cu_3O_{7-\delta}$ [5] and low-energy $\mu$SR data for optimally doped $YBa_2Cu_3O_{7-\delta}$ [5]. Triangles are torque magnetization and Meissner fraction data for $La_{2-x}Sr_xCuO_4$ [3; 4]. The lines correspond to the "differential Uemura" relation with $\Delta\lambda_{ab}(0)/\lambda_{ab}(0)=0.5|\Delta T_c/T_c|$ ("A"), $\Delta\lambda_{ab}(0)/\lambda_{ab}(0)=|\Delta T_c/T_c|$ ("B"), the "pseudo-gap" line from Ref. [7] ("C"), and the 2D-QSI relation given in Ref. [9] ("D"). The dashed lines indicate that the "differential Uemura" (line "A") and 2D-QSI (line "D") relations are strictly valid only in the under-doped regime (see Ref. [8]).**

Recently, we performed an OIE study on $T_c$ and $\lambda_{ab}(0)$ in optimally doped $La_{1.85}Sr_{0.15}CuO_4$ and $YBa_2CuO_{7-\delta}$, as well as in slightly under-doped $YBa_2Cu_4O_8$ and $Y_{0.8}Pr_{0.2}Ba_2Cu_3O_{7-\delta}$ by means of muon-spin rotation ($\mu$SR) (8). All the samples show a rather small OIE on $T_c$ associated with a relatively large OIE on $\lambda_{ab}(0)$ as shown in Fig. 8.1. The fact that a substantial OIE on $\lambda_{ab}(0)$ is observed even in cuprates having a relatively small OIE on $T_c$ suggests that lattice effects play an essential role in the occurrence of high-temperature superconductivity and have to be considered in any realistic model.


[1] J.P. Franck et al., Phys. Rev. B **44** 5318 (1991).

[2] D. Zech et al., Nature (London) **371**, 681 (1994).

[3] G.M. Zhao, M.B. Hunt, H. Keller, and K.A. Müller, Nature (London) **385**, 236 (1997).

[4] J. Hofer et al., Phys. Rev. Lett. **84**, 4192 (2000).

[5] R. Khasanov et al., J. Phys.: Condens. Matter **16**, S4439 (2004).

[6] H. Keller, in Superconductivity in Complex Systems, edited by K.A. Müller and A. Bussmann-Holder (Springer, Berlin 2005) p. 143.

[7] J.L. Tallon et al., Phys. Rev. Lett. **94**, 237002 (2005).

[8] R. Khasanov et al., Phys. Rev. B **74**, 064504 (2006).

[9] T. Schneider and H. Keller, New Journal of Physics **4**, 144 (2004).

### 8.1.2 Field dependence of oxygen isotope effects

The presence of nodes in the superconducting gap is probably one of the most significant features of cuprate HTS that has attracted considerable theoretical and experimental attention in recent years (see e.g., (1; 2)). The fourfold symmetric nature of the $d$-wave order parameter, together with the presence of gap nodes on the Fermi surface, open possibilities for novel effects to be observable in HTS. One of the most remarkable effect is the magnetic field dependence of the in-plane magnetic penetration depth $\lambda_{ab}$ observed in various HTS in the mixed state. It was shown that the field dependent correction to $\lambda_{ab}$ arises from the nonlocal and nonlinear response of a superconductor to an applied magnetic field (3; 4).

A simple analysis reveals that both the nonlinear and the nonlocal corrections to $\lambda_{ab}$ are expected to depend on the mass of the in-plane charge carriers $m^*_{ab}$ (5). A study of the field dependence of the isotope effect on $\lambda_{ab}$ can serve as a direct test of this prediction. Indeed, several OIE studies of the in-plane penetration depth $\lambda_{ab}$ in various cuprate families showed a pronounced oxygen-mass dependence of the in-plane supercarrier mass with ${}^{18}m^*_{ab} > {}^{16}m^*_{ab}$. Bearing in mind that within the simple London model $\lambda^2_{ab} \propto m^*_{ab}$ the in-plane magnetic penetration depth for the $^{16}$O substituted sample would increase stronger with increasing magnetic field than for the $^{18}$O substituted one.

We performed a study of the magnetic field dependence of the OIE on $\lambda_{ab}$ in $YBa_2Cu_4O_8$ and $Y_{1-x}Pr_xBa_2Cu_3O_{7-\delta}$ ($x$=0.2, 0.3) by means of $\mu$SR. The following results were obtained: For each pair of the $^{16}$O/$^{18}$O substituted samples $\lambda^{16}_{ab} < \lambda^{18}_{ab}$. The OIE on $\lambda_{ab}$ decreases by more than a factor of 2 with increasing magnetic field from $\mu_0 H$=0.2 T to $\mu_0 H$=0.6 T. Both findings may be explained by the isotope dependence of the in-plane charge carrier mass $m^*_{ab}$.


[1] D.J. Scalapino, Phys. Rep. **250**, 329 (1995).

[2] C.C. Tsuei et al., Phys. Rev. Lett. **73**, 593 (1994).

[3] M.H.S. Amin, M. Franz, and I. Affleck, Phys. Rev. Lett. **84**, 5864 (2000).

[4] M.H.S. Amin, Ph.D. thesis, University of British Colombia, (1999); cond-mat/0011455.

[5] R. Khasanov et al., Phys. Rev. B **75**, 060505 (2007).


## 8.2 Studies of pressure effects in novel superconductors

### 8.2.1 Pressure effect on the Ginzburg-Landau parameter $\kappa$ in $YB_6$

The Ginzburg-Landau parameter $\kappa = \lambda/\xi$ ($\lambda$ is the magnetic penetration depth and $\xi$ is the coherence length) is one of the fundamental parameters of a superconductor. The parameter $\kappa$ defines the border between type-I ($\kappa < 1/\sqrt{2}$) and type-II ($\kappa > 1/\sqrt{2}$) superconductors. Remarkably, the two physical quantities ($\lambda$ and $\xi$) entering $\kappa$ depend on different properties of the superconducting material. A simple analysis (1) reveals that $\lambda$(T=0) is determined by the *normal* state properties only, whereas $\xi$(T=0) depends on the *normal* and the *superconducting* state properties of the material. This means that if one is able to affect only the superconducting (normal) state properties of a superconductor, the Ginzburg-Landau parameter $\kappa$ would change. As a consequence, superconductors can be driven towards more type-I or more type-II behavior.

Experiments under pressure open a possibility to probe this phenomenon. It was shown (1) that the application of external pressure to an

$s-$wave BCS superconductor induces a large positive pressure effect (PE) on $\xi(0)$, together with a small positive effect on $\lambda(0)$, implying a strong negative pressure dependence of $\kappa(0)$. We studied the effect of pressure on the Ginzburg-Landau parameter $\kappa$ in the single-band isotropic BCS superconductor $YB_6$ (1). With increasing pressure from 0 to 9.18 kbar we observed a decrease of $\kappa(0)$ by almost 8%. The pressure effects on the two quantities ($\lambda(0)$ and $\xi(0)$) entering $\kappa(0)$ were studied separately. It was found that the PE on $\kappa(0)$ arises mostly from the pressure dependence of the coherence length $\xi(0)$, while no PE on the magnetic penetration depth $\lambda(0)$ (within the experimental accuracy) was observed. It was also noticed that in BCS superconductors for which the relative pressure shift of $T_c$ is much larger than $1/B$ ($B$ is the bulk modulus), the pressure shifts of the superconducting quantities such as $T_c$, $\kappa(0)$, $\xi(0)$, $H_{c2}(0)$, $dH_{c2}/dT|_{T=T_c}$ are related to each other (see Fig. 8.2).

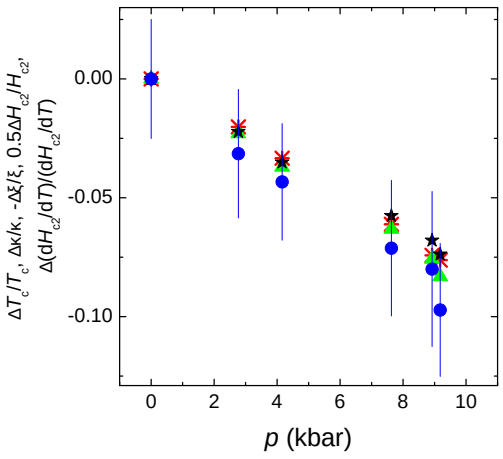


**Figure 8.2: Pressure dependences of the relative pressure shifts $\Delta T_c/T_c$ (red stars), $\Delta\kappa(0)/\kappa(0)$ (green triangles), $1/2\Delta H_{c2}(0)/H_{c2}(0)$ (black stars), and $\Delta(dH_{c2}/dT|_{T=T_c})/(dH_{c2}/dT|_{T=T_c})$ (blue circles) of the $YB_6$ superconductor.**

[1] R. Khasanov et al., Phys. Rev. Lett. **97**, 157002 (2006).

## 8.3 Spectroscopic studies of novel electronic materials

### 8.3.1 Charge effects in $LaBa_2Cu_3O_{7-\delta}$

We continued our search for charge effects in cuprates by means of $^{139}$La NMR/NQR on oriented $LaBa_2Cu_3O_{7-\delta}$ powder samples (1). La is sensitive to charge effects, since its nucleus carries an electric quadrupole moment and due to its site symmetry the magnetic fields from the antiferromagnetically correlated Cu spin fluctuations are canceled. From NQR measurements we have determined the electric field gradient at the La site (quadrupole frequency and asymmetry parameter).

At the $^{139}$La NMR central-line transition we determined the nuclear spin-lattice relaxation (NSLR) rate from 350 K down to 11 K. Above room temperature a thermally activated isotropic NSLR rate with an activation energy of the order of 2500 K was found. Below 270 K, however, a substantial rate anisotropy of 1.45 in the normal conducting phase was measured, which decreases below 200 K and becomes 1.3 below 150 K. By measuring the NSLR on corresponding satellite transitions at 100 K we found it to be independent of frequency, suggesting the interaction with conduction electrons as the main relaxation channel.

In the superconducting phase the NSLR rate for the field orientation parallel to the $c$ axis of the crystal drops (see Fig. 8.3a) without showing the expected pronounced rate maximum due to vortex dynamics as observed e.g. in investigations of Y NSLR in $YBa_2Cu_4O_8$ (2). The $^{139}$La nuclear spin-spin relaxation (NSSR) rate was measured by NMR at the central-line transition in the normal conducting phase. It is anisotropic in the whole investigated temperature range exhibiting pronounced steps and plateaus, which we confirmed in additional NQR NSSR measurements. To clarify the complex behavior of the measured

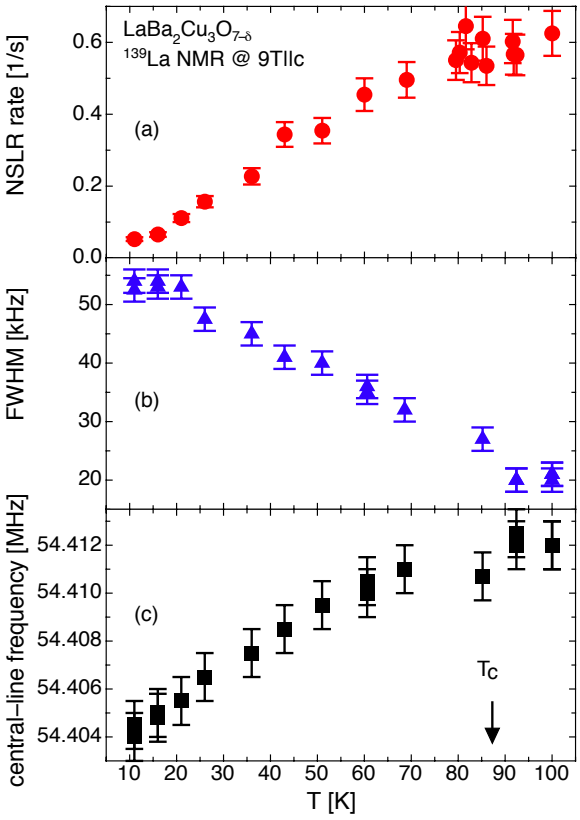


**Figure 8.3:**
**Temperature dependence of the nuclear spin-lattice relaxation rate (a), of the full line width at half maximum (b), and of the frequency position (c) of the central-line transition of $LaBa_2Cu_3O_{7-\delta}$ in the superconducting phase at 9 T parallel to the c axis.**

rates, further investigations are necessary. The $^{139}$La NMR central line in the superconducting phase shows a substantial increase of the line width with decreasing temperature (see Fig. 8.3b), reflecting the temperature behavior of the magnetic field inhomogeneity caused by the rigid vortex lattice. Moreover, a decrease of the frequency of the central line was observed (see Fig. 8.3c). It is a consequence of the onset of diamagnetism and the decrease of the positive Knight shift below $T_c$.

[1] S. Strässle et al., in press (Physica C).
[2] M. Corti et al., Phys. Rev. B **54**, 9469 (1996).

### 8.3.2 NQR investigations of Fe substituted $YBa_2Cu_4O_8$

The substitution of Cu atoms by other transition metal atoms, such as Fe, Zn, Ni, Co, have proved to be a powerful way to investigate the superconducting and normal state properties of cuprate HTS. In general, with increasing substitution $T_c$ is decreased progressively.

In case of the YBCO cuprate family the crystal structure has two different Cu sites: one in the chains (Cu1) with fourfold planar oxygen coordination, and the other (Cu2) in the $CuO_2$ planes with fivefold pyramidal coordination. It was observed that for Fe substitution in YBCO compounds the decrease of $T_c$ with increasing Fe content is much stronger in the underdoped stoichiometric compound $YBa_2Cu_4O_8$ than in $YBa_2Cu_3O_{7-\delta}$ (1; 2). Since superconductivity is mainly taking place in the electronic system of the $CuO_2$ planes, a simple explanation for this different behavior of the two compounds could be that in $YBa_2Cu_4O_8$ Fe replaces Cu(2) in the planes, whereas in $YBa_2Cu_3O_{7-\delta}$ it occupies Cu(1) sites in the chains. In the later case Fe substitution of Cu(1) was verified by several studies using various structural techniques (see e.g., Ref. (3; 4). For $YBa_2Cu_4O_8$ the experimental situation remained unclear. From $^{57}$Fe Mössbauer spectroscopy Bornemann et al. (2) and Boolchand et al. (3) found that Fe is replacing Cu(2) in the planes. In contradiction, Felner et al. (1) and Akachi et al. (5) using the same technique and additional X-ray-diffraction measurements observed Fe substituting Cu(1) in the chains.

In a new attempt to clarify this puzzling situation we performed Cu-NQR spectroscopy of $YBa_2(Cu_{1-x}Fe_x)_4O_{8+\delta}$ ( x = 0, 0.00625, 0.0125, 0.01875, 0.025, 0.05) using samples from the same source as used in the study of Ref. (5). Similar to the findings of Matsumura et al. (4) we observed a decrease of the integrated spectral intensity for both Cu sites with increas-

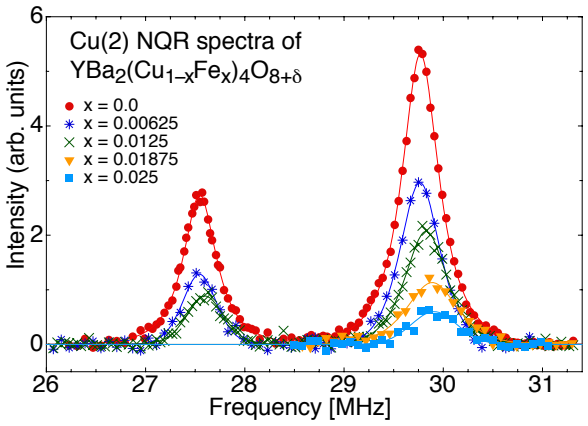


**Figure 8.4: Wipe-out of spectral intensity at the plane copper site Cu(2) of $YBa_2(Cu_{1-x}Fe_x)_4O_{8+\delta}$.**

ing x (wipe-out effect). The intensity from Cu nuclei that are neighbors (n, n.n or higher order n.n) to a Fe atom disappears from the observed spectra. Fig. 8.4 shows this fact for plane Cu(2). However, with growing x the intensity decrease is much stronger for Cu(2) than for Cu(1) in contrast to the case of Fe substituted $YBa_2Cu_3O_{7-\delta}$ (4). We performed various model calculations for a spectral wipe-out differing in site arrangements of Fe substitution and range of Cu neighbor order. The comparison with the observed x-dependent loss of spectral intensity for both Cu sites led us to the conclusion that Fe predominantly substitutes plane Cu sites especially for low Fe doping. We obtained additional strong support for these findings from the x-dependence of the spin-spin relaxation of the two Cu sites: whereas plane Cu(2) shows a remarkable growth of relaxation rate with increasing x, the relaxation of chain Cu(1) is independent of x. Furthermore, we observed in our investigation an influence of the extra oxygen introduced by Fe substitution on the long term microscopic structural stability of $YBa_2(Cu_{1-x}Fe_x)_4O_{8+\delta}$.

[1] I. Felner et al., Phys. Rev. B **43**, 8737 (1991).

[2] H.J. Bornemann et al., Physica C **199**, 130 (1992).

[3] P. Boolchand and D. McDaniel, in Studies on High-Temperature Superconductors, edited by Anant V. Narlikar (Nova Science, New Yoork, 1990, Vol. 4, p. 143.

[4] M. Masumura et al., Physica C **185-189**, 1135 (1991).

[5] T. Akachi et al., Physica C **301**, 315 (1998).

### 8.3.3 Study of charge transfer processes in Cr-doped $SrTiO_3$

During exposure to an electrical field (forming process), the resistance of Cr-doped $SrTiO_3$ is reduced by several orders of magnitude and a conductive state is reached. In this state electrical pulses of opposite polarity switch the resistance reversibly between a high- and a low-conductive state (1). We investigated the photocurrent induced at different wavelength in Cr-doped $SrTiO_3$. The illumination with photon-energy above 1.8 eV produces free electrons due to the ionization of $Cr^{3+}$. Such a valence state is possible in our crystals thanks to annealing in reducing atmosphere, and it explains why this charge transfer process is not visible in oxidized samples where the valence state of the Cr is $4^+$ (2). The photon excitation of one electron to the conduction band was observed by EPR measurements, which show a decrease of the $Cr^{3+}$ amount due to the light exposure. This process is fully reversible, and as shown in Fig.8.5(a), after 20 min in the dark the signal of $Cr^{3+}$ recovers to the initial value.

A completely different effect is visible by applying a bias of 100 V (Fig.8.5(b)). Even after removing the bias voltage and the light, after 20 min the signal does not recover. This is a clear effect of the bulk change induced by the electric field, which modified the recovery process of $Cr^{3+}$. By combining EPR, with in-situ I-V measurements we found that the increase of the electrical current is correlated with the

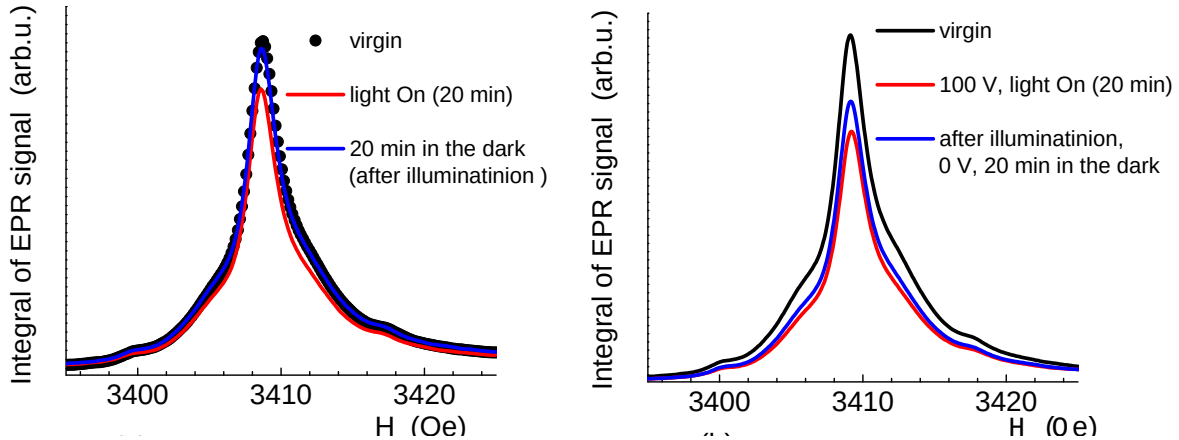


**Figure 8.5: EPR signal of $Cr^{3+}$ in Cr-doped $SrTiO_3$ at different photo-excitation (white light).**

decrease of the $Cr^{3+}$ EPR signal. The exposure to white light produces a photocurrent that decreases the forming time. One possible explanation is that the photo-ionization of the $Cr^{3+}$ enhances the current which produces some avalanche processes leading to the insulator-to-metal transition.

### 8.3.4 Oxygen isotope effect of the spin-lattice relaxation of $Yb^{3+}$ in Yb substituted $YBa_2Cu_3O_{7-\delta}$

Recently we performed a detailed study of the temperature dependence of $Yb^{3+}$ relaxation in $YBa_2Cu_3O_x$ by measuring the $Yb^{3+}$ EPR linewidth (1). It was found that both electronic and phononic processes contribute to $Yb^{3+}$ relaxation. We were able to separate these processes and studied their relative contributions to relaxation as a function of oxygen doping. As expected, the electronic contribution decreases with decreasing oxygen doping, while the phonon contribution is practically doping independent. Note

[1] A. Beck et al., Appl. Phys. Lett. **77**, 139 (2000).
[2] S. A. Basun et al., Ferroelectrics **183**, 255 (1996).

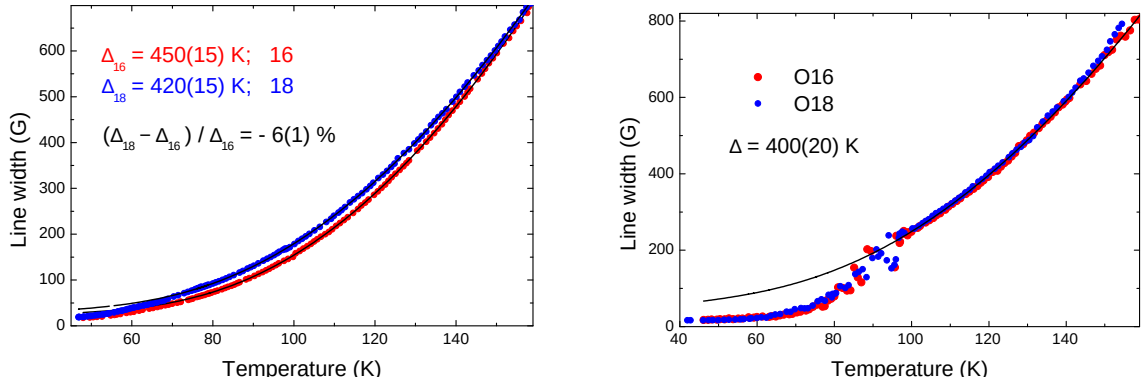


**Figure 8.6: Temperature dependence of the $Yb^{3+}$ EPR linewidth (relaxation rate) for $^{16}O$ and $^{18}O$ samples of underdoped $Y_{0.98}Yb_{0.02}Ba_2Cu_3O_{6.6}$ (left panel) and optimally doped $Y_{0.98}Yb_{0.02}Ba_2Cu_3O_{6.95}$ (right panel).**

that traditional Raman and Orbach mechanisms involving acoustic phonons cannot explain the temperature dependence of the $Yb^{3+}$ EPR linewidth. Instead, it appears that a Raman process via the coupling to high-energy ($\sim$ 500 K) optical phonons is responsible for the phononic part of $Yb^{3+}$ relaxation in $YBa_2Cu_3O_x$. In this case one can expect an oxygen isotope effect (OIE) on $Yb^{3+}$ relaxation. We checked this possibility by studying the $Yb^{3+}$ EPR linewidth in $YBa_2Cu_3O_x$ with different oxygen isotopes ($^{16}O$ and $^{18}O$).

Two samples with different oxygen concentrations, $x$=6.6 (under-doped) and 6.95 (optimally doped) were studied. Figure 8.6 shows the temperature dependence of the EPR linewidth of these oxygen exchanged ($^{16}O$ and $^{18}O$) samples. In the under-doped sample there is a clear OIE on the EPR linewidth. On the other hand, no OIE is observed in the optimally doped sample. Surprisingly, the OIE on the $Yb^{3+}$ EPR linewidth behaves very similar as the OIE on $T_c$, which is large in the under-doped regime and very small at optimal doping.

[1] Annual Report 2005/2006, www.physik.unizh.ch/reports.html.

### 8.3.5 $\mu$SR study of the non-centrosymmetric superconductors $Li_2(Pt, Pd)_3B$

Recently, the non-centrosymmetric superconductors $Li_2Pd_3B$ and $Li_2Pt_3B$ were discovered (1; 2). Some experiments indicate a parity-mixed superconducting state, in particular a significant spin-triplet contribution in $Li_2Pt_3B$ (3; 4), while others suggest both compounds to be BCS-type superconductors with an isotropic gap (2). Further evidence for s-

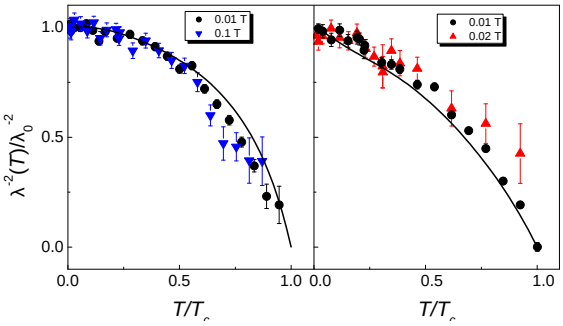


**Figure 8.7: $\lambda^{-2}$(T)/$\lambda^{-2}$(0) versus reduced temperature T/$T_c$ for $Li_2Pd_{1.5}Pt_{1.5}B$ (left panel) and $Li_2Pt_3B$ (right panel) at different applied fields. The solid lines correspond to a theoretical fit as explained in the text.**

wave superconductivity in $Li_2Pd_3B$ stems from our previous studies (5). In order to elucidate this controversy, we investigated $Li_2Pd_{1.5}Pt_{1.5}B$ and completely Pt substituted $Li_2Pt_3B$ by means of the transverse-field $\mu$SR technique.

Figure 8.7 shows the temperature dependence of the magnetic penetration depth $\lambda$ normalized to the value at zero temperature $\lambda$(0), i.e. the quantity $\lambda^{-2}(T)/\lambda^{-2}$(0), for the samples studied. $\lambda^{-2}(T)/\lambda^{-2}$(0) saturates at low temperatures for $Li_2Pd_{1.5}Pt_{1.5}B$ (left panel), which is expected for an isotropic superconductor, whereas in $Li_2Pt_3B$ (right panel) the slope of $\lambda^{-2}(T)/\lambda^{-2}$(0) is nonzero in the low-temperature regime, probably suggesting the existence of nodes in the superconducting gap.

In general the lack of inversion symmetry induces an antisymmetric spin orbit coupling (ASOC), which is not destructive to special spin-triplet states. As a consequence an admixture of spin-singlet and spin-triplet states are allowed. The ASOC lifts the energy degeneracy of the spin states and results in a two-gap function where nodes may exist in one gap depending on the weight of the spin triplet contribution. We analyzed our $\mu$SR data based on these ideas (solid lines in Fig. 8.7) using the BCS expression for $\lambda^{-2}(T)/\lambda^{-2}$(0) under the assumption of two anisotropic gaps

whose expression was elaborated in Ref. (3). We obtain a dominant spin triplet contribution in $Li_2Pt_3B$ in agreement with Ref. (3), whereas $Li_2Pd_{1.5}Pt_{1.5}B$ seems to be a fully gapped superconductor like $Li_2Pd_3B$ (5). These findings are also consistent with an increasing spin-orbit coupling with growing Pt content (6).


[1] K. Togano et al., Phys. Rev. Lett. **93**, 247004 (2004).

[2] H. Takeya et al., Phys. Rev. B **72**, 104506 (2005).

[3] H.Q. Yuan et al., Phys. Rev. Lett. **97**, 017006 (2006).

[4] M. Nishiyama et al., Phys. Rev. Lett. **98**, 047002 (2007).

[5] R. Khasanov et al., Phys. Rev. B **73**, 214528 (2006).

[6] K.-W. Lee and W.E. Pickett, Phys. Rev. B **72**, 174505 (2005).


### 8.3.6 Investigation of the two-gap behavior of $La_{2-x}Sr_xCuO_4$

It is mostly believed that the order parameter in cuprate HTS has pure $d-$wave symmetry, as indicated by e.g. tri-crystal experiments (1). There are, however, a wide variety of experimental data that support $s$ or even more complicated types of symmetries ($d+s$, $d+is$, etc.) (2). In order to solve this controversy Müller suggested the presence of two superconducting condensates with different symmetries ($s-$ and $d-$wave) in HTS (3). This idea was generated partly because two gaps were observed in $n-$type $SrTiO_3$ (4), the first oxide in which superconductivity was detected. In addition, it is known that a two-order parameter scenario leads to a substantial increase of the superconducting transition temperature in comparison to a single-band model (5).

Important information on the symmetry of the order parameter can be obtained from magnetic field penetration depth $\lambda$ measurements. Recently, we performed a study of the in-plane magnetic penetration depth ($\lambda_{ab}$) in slightly over-doped single-crystal $La_{1.83}Sr_{0.17}CuO_4$ by means of $\mu$SR (6). At low magnetic fields ($\mu_0 H < 0.3$ T), $\lambda_{ab}^{-2}(T)$ exhibits an inflection point at $T \approx$10-15 K (see Fig. 8.8). We interpret this feature as a consequence of the presence of two superconducting gaps, analogous to double-gap $MgB_2$ (7). It is suggested that the large gap ($\Delta_1^d$=8.2(1) meV) has $d-$ and the small gap ($\Delta_2^s$=1.57(8) meV) $s-$wave symmetry. With increasing magnetic field the contribution of $\Delta_2^s$ decreases substantially, in contrast to an almost constant contribution of $\Delta_1^d$. Both the temperature and the field dependencies of $\lambda_{ab}^{-2}$ were found to be similar to what was observed in double-gap $MgB_2$ (7; 8).

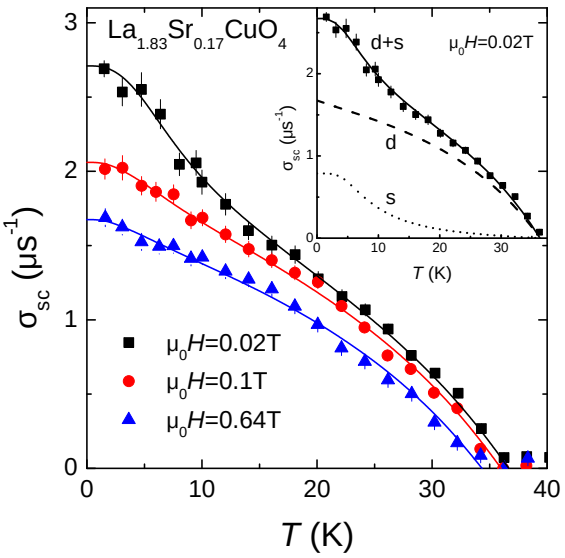


**Figure 8.8: Temperature dependence of the $\mu$SR relaxation rate $\sigma_{sc} \propto \lambda^{-2}_{ab}$ of single-crystal $La_{1.83}Sr_{0.17}CuO_4$ measured at 0.02 T, 0.1 T, and 0.64 T (field-cooled). Lines in the main figure and in the inset represent the fit with the two-gap model [6]. In the inset the contributions from the large d-wave gap and the small s-wave gap at $\mu_0$H=0.02 T are shown separately.**

[1] C.C. Tsuei et al., Phys. Rev. Lett. **73**, 593 (1994).
[2] G. Deutscher, Rev. Mod. Phys. **77**, 109 (2005).
[3] K.A. Müller, Nature (London) **377**, 133 (1995).
[4] G. Binnig et al., Phys. Rev. Lett. **45**, 1352 (1980).
[5] A. Bussmann-Holder et al., Eur. Phys. J. B **37**, 1434 (2004).
[6] R. Khasanov et al., Phys. Rev. Lett **98**, 057007 (2007).
[7] A. Carrington and F. Manzano, Physica C **385**, 205 (2003).
[8] S. Serventi et al., Phys. Rev. Lett. **93**, 217003 (2004).

## 8.4 Magnetic properties of novel electronic materials

### 8.4.1 Study of the upper critical field anisotropy of $Al_{0.16}Mg_{0.84}B_2$

It is now well accepted that $MgB_2$ is a conventional phonon mediated superconductor, with the peculiarity to have two separate gaps, whose interplay strongly influences the physical properties of the material. The temperature dependence of the upper critical field anisotropy $\gamma_H = H_{c2}^{||ab}/H_{c2}^{||c}$, first observed by (1), can be understood as the changing interplay of the two bands by varying the temperature.

Recently, much progress in understanding the superconducting properties of this two-band superconductor was made by doping aluminum into $MgB_2$ single crystals. Whereas $T_c$ decreases by replacing the Mg ions with aluminum, point-contact spectroscopy studies show that the two-gap behavior remains up to 20% doping (2).

By using the combination of a magnetic torque magnetometer with highly sensitive piezo-resistive sensors and a commercial SQUID (Quantum Design MPMS XL) we studied how the anisotropy evolves with temperature and heavy aluminum doping. In Fig. 8.9 the measured temperature behavior of $\gamma_H$ and the upper critical field $H_{c2}$, which strongly depends on the direction of the field relative to the crystallographic axes, of $Al_{0.16}Mg_{0.84}B_2$ and pure $MgB_2$ is shown. While $\gamma_H$ of $MgB_2$ is strongly temperature dependent, the anisotropy of $Al_{0.16}Mg_{0.84}B_2$ is much reduced compared to $MgB_2$ and is almost temperature independent. This suggests that the two-gap behavior becomes less important with higher Al doping.

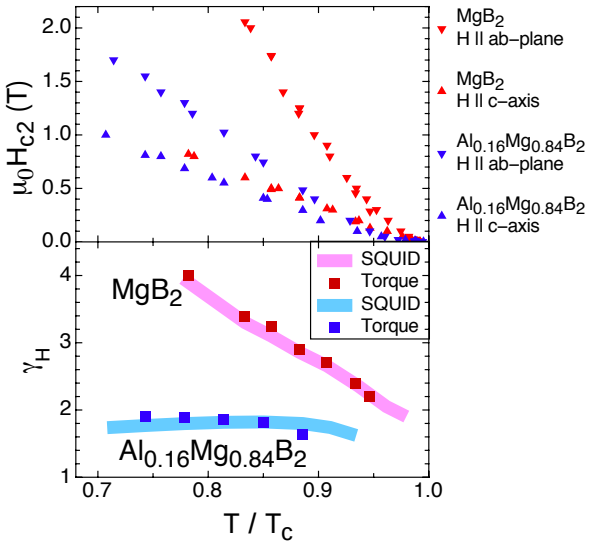


**Figure 8.9: Upper graph: Temperature dependence of $H_{c2}^{||c}$ and $H_{c2}^{||ab}$ of $MgB_2$ and $Al_{0.16}Mg_{0.84}B_2$ measured by torque and SQUID magnetometry. Lower graph: Temperature dependence of upper critical field anisotropy $\gamma_H$ of $MgB_2$ and $Al_{0.16}Mg_{0.84}B_2$. The anisotropy of $Al_{0.16}Mg_{0.84}B_2$ is clearly reduced and almost temperature independent.**

[1] M. Angst et al., Phys. Rev. Lett. **88**, 167004 (2002).
[2] J. Karpinski et al., Phys. Rev. B **71**, 174506 (2005).

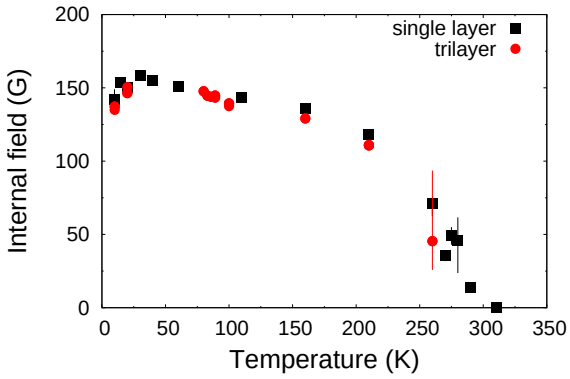


**Figure 8.10: Spontaneous internal fields in PBCO (black squares: single layer 50 nm, red circles: tri-layer) as a function of temperature.**

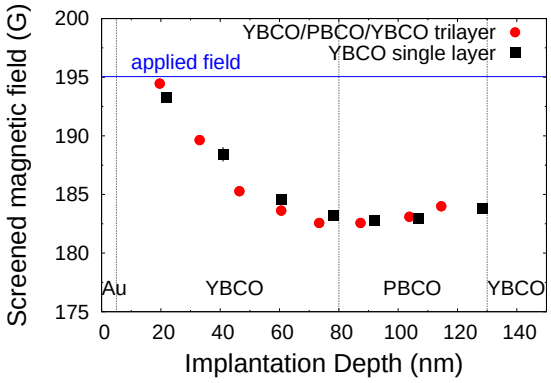


**Figure 8.11: The diamagnetic field profile measured inside the tri-layer at T=25 K (circles) and the 200 nm YBCO single layer (squares).**

### 8.4.2 Low-energy $\mu$SR experiments on multilayers

Proximity effects in multilayers have been subject of intense research in recent years due to the variety of phenomena resulting from the interplay (competition and coexistence) between the two orderings in hetero-structures. For instance in super-lattices consisting of one unit cell thick layers of $YBa_2Cu_3O_7$ (YBCO) separated by $PrBa_2Cu_3O_7$ (PBCO) layers of variable thickness, the critical temperature of the heterostructure has been found to continuously decrease as the PBCO thickness is increased, indicating that some sort of coupling persists over distances of $\sim$10 nm (1).

Polarized low energy muons implanted in a YBCO(75nm)/PBCO(50nm)/YBCO(75nm) trilayer were used to investigate the local superconducting and magnetic properties of this structure. For comparison we investigated also single layer films of the constituents. Figure 8.10 shows the internal field measured by zero-field $\mu$SR in the PBCO layer as single film (50nm) and embedded in the two YBCO layers. Both samples show similar internal field distributions. If an external magnetic field is applied parallel to the surface (and perpendicular to the c-axis), by scanning the implantation energy, one can probe the field distribution of the YBCO layers in the Meissner state and the local magnetic field inside the PBCO layer. Superconductivity of YBCO manifests itself in a screened diamagnetic signal. In PBCO, the microscopic field measurements show two components. The first component reflects the magnetic order and appears at fields corresponding to the superposition of the internal and external fields. The second component displays a sizeable diamagnetic shift below the critical temperature of YBCO. The depth profile of the diamagnetically shifted component exhibits a monotonic decay in the YBCO layer and reaches the maximum shift in the PBCO layer (Fig. 8.11). Moreover, it is close to the field profile inside the 200 nm YBCO single layer in the Meissner state plotted for comparison. This result may present the signature of a large proximity effect not expected in this material on the base of conventional proximity models.

[1] J.M. Triscone and Ø. Fischer, Rep. Prog. Phys. **60** 1673 (1997).

### 8.4.3 $\mu$SR study of magnetic semiconductors

Recently, high temperature ferromagnetism was observed in chalcopyrite semiconductors doped by Mn, namely in CdGeP2:Mn, ZnGeP2:Mn, ZnGeAs2:Mn, and CdGeAs2:Mn (1), where the record Curie temperature of 350 K was reported. These novel diluted ferromagnetic semiconductors (DMS) are believed to be promising for room temperature spintronics. Our first $\mu$SR measurements at PSI of $CdGeAs_2$ polycrystalline samples doped with Mn (2) confirmed that the ferromagnetism detected in these samples is a bulk phenomenon, and revealed a big shift of the magnetic field seen by the muon. To understand the nature of this shift one has to appreciate the origin of the net magnetic field seen by the muon in a ferromagnetic medium according to the concept of a Lorentz sphere (3):

$$B_\mu = B_{ext} - B_{dem} + B_L + B_c + B_{dip},$$

where $B_{ext}$ is the external magnetic field; $B_{dem} = 4\pi N m$ ($N$ - demagnetization factor of the sample, $m$ - magnetization) and $B_L = \frac{4\pi}{3} m$ are demagnetization fields from the finite sample and the empty Lorentz sphere ($N_{sphere} = \frac{1}{3}$), respectively; $B_c$ is the contact hyperfine field at the muon and $B_{dip}$ is the net magnetic field from magnetic dipoles inside the Lorentz sphere. In the case of a rectangular sample (8x8 $mm^2$, thickness 0.82 mm) (2), the uncertainty of $N$ introduced a large systematic error in the determination of the physical term $B_c + B_{dip}$.

To eliminate this uncertainty experiments must be performed with spherical samples ($N = \frac{1}{3}$), where the Lorentz field and demagnetization field cancel each other. This year we were able to get a big polycrystalline sample of $CdGeAs_2$:3%Mn and to machine it to an almost spherical shape (diameter 3.30(5) mm).

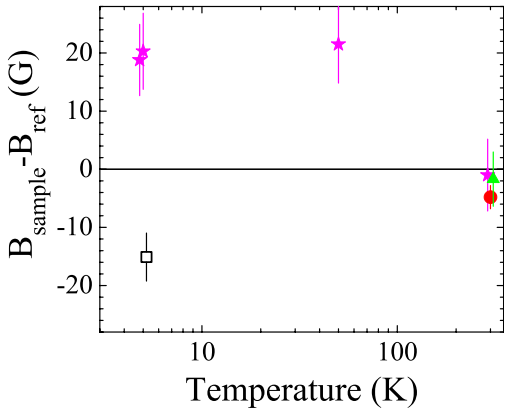


**Figure 8.12: Temperature dependence of the field shift seen by the muon in $CdGeAs_2$ doped with 3% Mn. The applied field is H=6400 Oe. Different symbols correspond to the different orientations of the sample. Circle - original position; triangle - sample rotated 60°; square - sample rotated 180°; stars - sample rotated -60°.**

Fig. 8.12 shows the difference between the field seen by the muon and the applied field of 6400 Oe as a function of temperature. To eliminate the systematic errors due to unideal shape, several measurements with different sample orientations have been conducted. At room temperature the data points are scattered with an average value $dB$ =-1.6±1.5 G. The measured value of $B_c + B_{dip}$ is about 3-4 orders of magnitude less than that in ferromagnetic metals Fe, Co, Ni, Gd etc. (3). This value has to be set against theoretical estimates using recent calculations (4; 5; 6).

[1] V.M. Novotortsev et al., Rus. J. Inorg. Chem. **50**, 492 (2005).

[2] V.G. Storchak et al., Physica **B374-375**, 430 (2006).

[3] A. Schenck, Muon Spin Rotation: Principles and Applications in Solid State Physics, Adam Hilger, Bristol, 1986.

[4] S.C. Ervin and I. Zutic, Nature Materials **3**, 410 (2004).

[5] Y.-J. Zhao, W.T. Geng, A.J. Freeman, and T. Oguchi, Phys. Rev.**B63**, 201202 (2001).

[6] P. Mahadevan and A. Zanger, Phys. Rev. Lett. **88**, 047205 (2002).

## 8.5 Electric field effects in perovskites

### 8.5.1 Resistive memory effects in Cr-doped $SrTiO_3$

Resistive memory effect (resistive switching) in some selected perovskites are under intense investigation because of their potential technological applications for non-volatile memory devices. We report on a study of single crystals of Cr-doped $SrTiO_3$ as a model system (1). By comparing the EPR signal in the insulating state and the conducting state obtained after exposure to an electrical field (forming), a broadening of the lineshape of the $Cr^{3+}$ signals was detected after the forming process. Such changes indicate that the forming procedure affects a volume fraction of $\leq 10\%$ of the entire bulk. By optical measurements during the forming process, while applying positive and negative voltage pulses, we were able to detect a luminescence band centered at 790nm. This luminescence is known as the Cr R-line (2) resulting from a recombination of electrons at the $Cr^{4+}$ center, and is a clear signature of a charge transfer process involved during the insulator-to-metal transition. A broader band was detected at the same spectral region during the memory switching from the high to the low conductive state which indicates that a carrier recombination process occurs during the resistance increase. Additional investigations are required to assign the broad luminescence line to well defined energy level of the Cr-doped $SrTiO_3$.

[1] Y. Watanabe et al., Appl. Phys. Lett. **78**, 3738 (2001).

[2] T. Feng, Phys. Rev. B **25**, 627 (1982).

### 8.5.2 $\mu$SR study of conductive Cr-doped $SrTiO_3$

Knowledge about the role of oxygen vacancy doping in $SrTiO_3$ is essential in order to understand the physics of the insulator-to-metal transition in the material. Muon-spin rotation experiments (including $\mu$SR in electric fields) proved to be a powerful tool to study muonium (muon + electron) and other muon charge states in semiconductors and insulators. Usually muonium is detected in insulators or slightly doped semiconductors, whereas bare muons are observed in heavily doped semiconductors and metals. Monitoring the ratio muon to muonium signal intensity can yield an estimate of the metal to insulator volume ratio. Transverse magnetic field $\mu$SR measurements on a single crystal of Cr-doped $SrTiO_3$ shows a change in the muon signal (asymmetry) due to a different annealingprocedure of the virgin materials (Fig.8.13).

We found the largest muon signal in the virgin oxygen vacancy enriched sample (black).

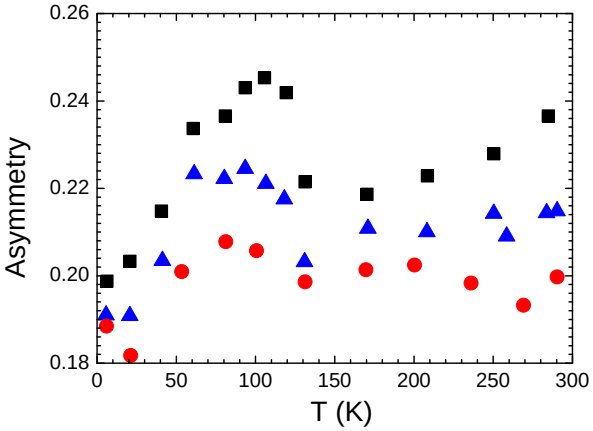


**Figure 8.13: Temperature dependence of the asymmetry parameter of single crystal $SrTiO_3$:Cr0.2%.**

**black:** **virgin reduced (annealed in $H_2$/Ar:5% at 1150°C for 8h)**

**red:** **virgin oxidized (annealed in $O_2$ at 1150 °C for 8h)**

**blue:** **reduced conductive**

The two annealing procedures affect both the Cr valence state and the oxygen vacancy content due to a charge compensation. By comparing the two virgin samples one can conclude that in the virgin oxygen vacancy enriched sample the larger muon signal reflects a larger metallic volume fraction. On the other hand, a decrease of the muon signal in the conducting state obtained after the electric field forming procedure is in contradiction to the idea of an increase of the fraction of metallic regions. This observation requires more experimental investigations.

## 8.6 New developments in instrumentation and data handling

### 8.6.1 Implementation of the flip-coil technique at the Avoided Level Crossing instrument at PSI

In avoided level crossing (ALC) experiments the integral muon decay asymmetry

$$Asy = (F - B)/(F + B)$$

(where $F$ and $B$ are the total number of positron events in the forward and backward counters, respectively) is measured as a function of applied magnetic field. One principal limitation of a standard ALC technique lies in the systematic fluctuations due to the various beam line instabilities (noise of the power supplies, fluctuation of the primary proton beam, small HV discharges in the separator). Typical clean and noisy raw ALC spectra are presented in Fig. 8.14. To average out systematic errors the so-called flip-coil technique was introduced at TRIUMF (1). A similar approach (Red-Green mode) is used at ISIS.

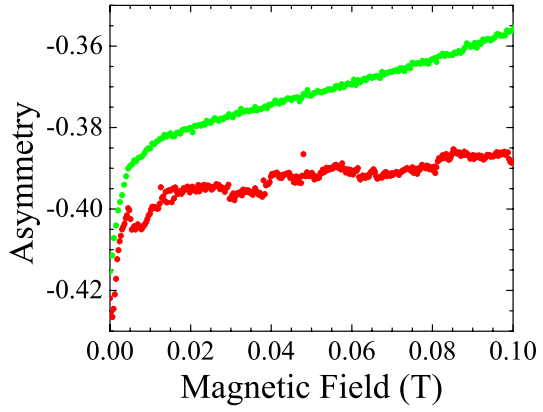


**Figure 8.14: Typical examples of a clean (green) and a noisy (red) raw ALC spectrum.**

Here we report the first implementation of the flip-coil technique at the ALC instrument at PSI. A small coil capable to produce a square-wave modulation field (amplitude up to $\Delta H$ $\simeq$20 Oe) was attached to the standard ALC cryostat and placed inside the warm bore of the superconducting magnet. The modulation field was alternated at a frequency of 1 Hz by an external generator and two separate ALC spectra were collected

$$Asy^{\pm} = (F^{\pm} - B^{\pm})/(F^{\pm} + B^{\pm}),$$

where $\pm$ refers to the direction of the modulation field. Finally, one can construct the differential asymmetry

$$Asy_{\rm diff} = Asy^{+} - Asy^{-}$$

or

$$Asy(H)_{\rm diff} = Asy(H + \Delta H/2) - Asy(H - \Delta H/2).$$

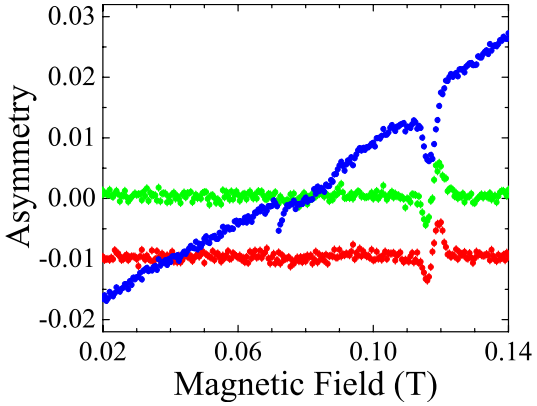


**Figure 8.15: ALC spectra measured in $Al_2O_3$ at T=15 K in an electric field E=+11.32 kV/cm.**
**Red - Asy$_{diff}$ of "clean" data (shown shifted by -0.01 for clarity).**
**Blue - noisy original raw signal.**
**Green - Asy$_{diff}$ made of the original noisy signal.**
**One can see that the noise is absent in the flip-coil presentation.**

For low frequency fluctuations ($f_{\rm noise} < 1$ Hz) the noise contribution to $Asy_{\rm diff}$ is subtracted. These features are illustrated in Fig 8.15. In conclusion, the flip-coil technique was implemented at the ALC instrument and is ready for further experiments.

[1] R.F. Kiefl et al., Phys. Rev. **A34**, 681 (1986).

### 8.6.2 Setup for simultaneous observation of EPR, luminescence and current-voltage measurements

In order to study changes in the valence states of transition metal ion dopants (Cr, Fe, Co, Mn) in $SrTiO_3$ during current voltage (I-V) measurements, a special sample holder and special electrodes were developed. Simultaneous measurements of EPR, I-V curves, and luminescence are now possible with a reproducibility of the EPR signal improved from 10% to 1%, which is an essential prerequisite to study small changes in the entire bulk. The new setup (Fig.8.16 ) consist of a special enlarged hole window in the wall of the EPR cavity which is aligned with a series of two optical lenses. The sample position coincides with the center of the cavity and the focal point of the first lense. With such a system it is possible to collect light emitted by the sample and couple it to an optical fiber connected to a Single Photon Counting Module (SPCM of Laser Components) with a dark count of 25 cps. The SPCM is then connected to a ratemeter (Canberra Lin-Log Ratemeter 1481LA). For the I-V in-situ measurement stripe-like electrodes of platinum are deposited on two opposite faces of the $SrTiO_3$ single crystal. Such stripe-like platinum layers being transparent to the EPR microwave allow to apply an electrical field and give access for the optical luminescence detection.

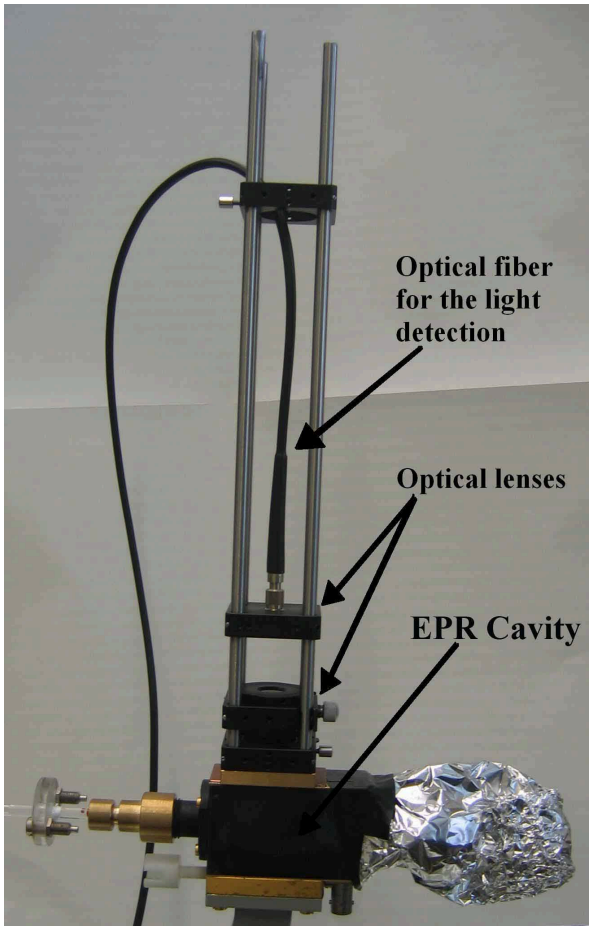


**Figure 8.16: EPR cavity modified for optical luminescence detection.**

### 8.6.3 Calculation of the magnetic field distribution in type-II superconductors

Analysis of $\mu$SR data for type-II superconductors with a high value of $\kappa = \lambda/\xi$, like cuprate HTS, is a demanding task. In this case the second moment of the magnetic field distribution in the mixed phase depends on several parameters: the penetration depth $\lambda$, the coherence length $\xi$, and the degree of the vortex lattice disorder (1). Several methods were proposed to calculate $\mu$SR spectra as a function of these parameters (see for example (2)). However, most of them fail to describe precisely experimental data

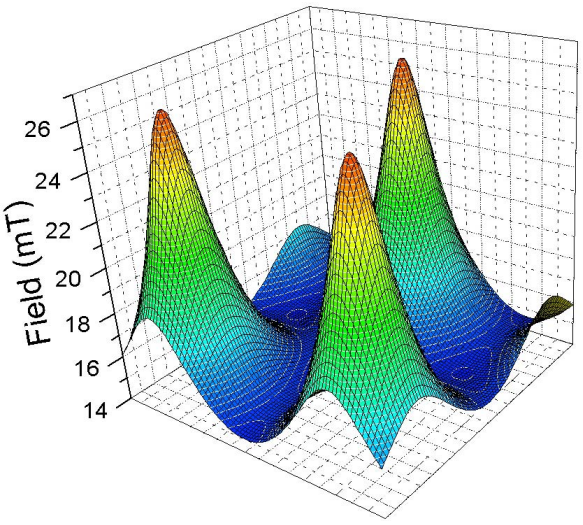


**Figure 8.17: Spatial distribution of the magnetic field in a type-II superconductor calculated using the Ginzburg-Landau model for $\lambda$ = 200 nm, $\xi$ = 20 nm, average field 0.02 $\mu_0 H_{c2}$ = 16.45 mT, and inter-vortex distance 380.9 nm.**

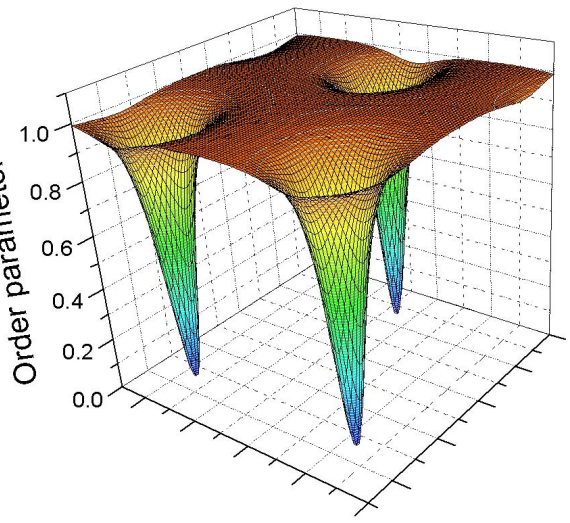


**Figure 8.18: Spatial distribution of the normalized absolute value of the order parameter in a type-II superconductor calculated using the Ginzburg-Landau model for $\lambda$ = 200 nm, $\xi$ = 20 nm, average field 0.02 $\mu_0 H_{c2}$ = 16.45 mT, and inter-vortex distance 380.9 nm.**

as the applied magnetic field approaches $H_{c2}$. The magnetic field distribution in a flux line lattice (FLL) can be calculated using the Ginzburg-Landau model. Brandt described an algorithm for numerical calculation of the magnetic field distribution in a type-II superconductor for hexagonal and rectangular geometries of the FLL by minimizing the Ginzburg-Landau free energy (3). Based on this algorithm we wrote a program in MATLAB to simulate and to fit the field and time domain $\mu$SR spectra.

As an example, Figs. 8.17 and 8.18 show the spatial distribution of the magnetic field and the order parameter of a type-II superconductor, calculated by our program. The corresponding field domain $\mu$SR spectrum is shown in Fig. 8.19. Compared to other models the program is able to analyze type-II superconductors with small values of $\kappa$ and in fields close to $H_{c2}$. It also allows the exact calculation of the reversible magnetization in type-II superconductors.

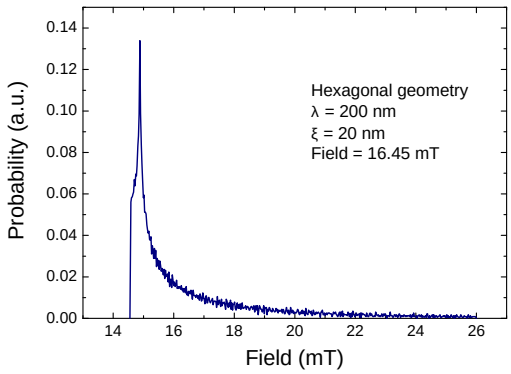


**Figure 8.19: Field domain $\mu$SR spectrum corresponding to the spatial distribution of magnetic field shown in Fig. 8.17**

[1] E.H. Brandt, Phys. Rev. B, **68**, 054506 (2003).

[2] J.E. Sonier, J.H. Brewer, and R.F. Kiefl, Rev. Mod. Phys., **72**, 769 (2000).

[3] E.H. Brandt, Phys. Rev. Lett., **78**, 2208 (1997).